QUANTIFYING INTRA-CANOPY HYPERSPECTRAL HETEROGENEITY WITH RESPECT TO SOYBEAN ANATOMY

by

Samantha Neeno

A Thesis

Submitted to the Faculty of Purdue University

In Partial Fulfillment of the Requirements for the degree of

Master of Science in Agricultural and Biological Engineering

School of Agricultural and Biological Engineering

West Lafayette, Indiana

May 2020

THE PURDUE UNIVERSITY GRADUATE SCHOOL
STATEMENT OF COMMITTEE APPROVAL

Dr. Jian Jin

School of Agricultural and Biological Engineering

Dr. John Couture

School of Entomology and Forestry and Natural Resources

Dr. Jeffrey Volenec

School of Agronomy

Dr. Shweta Singh

School of Agricultural and Biological Engineering

Dr. Somali Chaterji

School of Agricultural and Biological Engineering

Approved By:

Dr. Nathan S. Mosier

Dedicated to my loves across the country.
Your courage inspires me, every day.
I am lucky to have you.

ACKNOWLEDGMENTS

TABLE OF CONTENTS

LIST OF TABLES

LIST OF FIGURES

ABSTRACT

To support the growing human population, plant phenotyping technologies must innovate to rapidly interpret hyperspectral (HS) data into genetic inferences for plant breeders and managers. While pigment and nutrient concentrations within canopies are known to be vertically non-uniform, these chemical distributions as sources of HS noise are not universally addressed in scaling leaf information to canopy data nor in detecting spectral plant health traits.

In this project, soybeans (*Glycine Max,* cultivar Williams 82) were imaged with a Spectra Vista Corporation (SVC) HR-1024 spectroradiometer (350-2500 nm) at the highest five node positions. The samples were subjected to nitrogen and drought stress in factorial design (n=12) that was validated via relative water content (RWC) and PLS Regression of photopigments (chlorophyll a, chlorophyll b, lutein, neoxanthin, violaxanthin, and zeaxanthin in mg/g DW) and N concentration (%) for each imaged tissue. Welch's ANOVA and Tamhane's T2 post-hoc testing quantified spectral heterogeneity with respect to treatments and node positions through spectral angle measurements (SAMs) and percent NDVI difference. Drought-stressed samples had the lowest SAM between node positions compared to other treatments, and SAM node comparisons were greatest when including the highest sampled tissues. Taking ratios of NDVI between node positions proved more statistically effective at discerning between all factorial treatments than individual leaf NDVI values. Finally, intra-canopy spectral heterogeneity was exploited by training Linear Discriminant Analysis (LDA) classifiers on relative reflectance between node positions, tuning for the F1-Score. A classifier built on Node 1 vs. Node 3 reflectance outperformed in class-specific accuracies compared to analogous models trained on point-view data. Accounting for intra-canopy spectral variability is an opportunity to develop more comprehensive phenotyping tools for plant breeders in a world with rapidly rising agricultural demand.

1. INTRODUCTION

Agricultural management techniques and plant phenotyping must innovate to accommodate the needs of a 9.7 billion human population in time for 2050 (DESA, 2019; Walter, Finger, Huber, & Buchmann, 2017). Plant phenotyping aims to measure the manifestation of genomes with respect to their environments, with particular attention to traits supporting yield and stress resistance (Pieruschka & Schurr, 2019; Poorter et al., 2012). Hyperspectral imaging (HSI) techniques have delivered the benefits of radiometers' spectral resolution in addition to spatial data, evolving into a potent tool for plant phenotyping over the past decades (Curran, Dungan, & Peterson, 2001; Fahlgren, Gehan, & Baxter, 2015; Fiorani & Schurr, 2013; L. Li, Zhang, & Huang, 2014; Mahlein, Kuska, Behmann, Polder, & Walter, 2018). One of plant phenotyping's acute challenge is linking imaging and spectral data collected from varying resolutions (leaf, canopy, etc…) to actionable genetic information (Furbank & Tester, 2011; Minervini, Scharr, & Tsaftaris, 2015; Mochida et al., 2018).

HS data can permit nondestructive inferences on targets' chemical profiles, a crucial feature to monitoring crops over seasons. Absorptions features at specific wavelengths are used to generate vegetative indices (VIs) that contain information on water content (Gao, 1996; Tilling et al., 2007), photochemical concentrations such as chlorophylls, carotenes, and xanthophylls (Blackburn, 2007; Gamon & Surfus, 1999; Haboudane, Miller, Pattey, Zarco-Tejada, & Strachan, 2004; Peñuelas, Josep; Filella & Gamon, 1995; Sims & Gamon, 2002; Yoder & Pettigrew-Crosby, 1995), and structural chemicals such as lignin (Green et al., 1998; Kokaly, Asner, Ollinger, Martin, & Wessman, 2009). The Normalized Difference Vegetation Index (NDVI) is a ubiquitous example, which is frequently used to represent general vegetative health (Fischer et al., 1998). However, many VIs exist that are correlated to specific changes in pigment concentrations indicative of environmental stresses (Altangerel et al., 2017). High dimensional spectra are also examined with spectral angle measurements (SAM) (Kruse et al., 2008), signal derivatives (Le Maire, François, & Dufrêne, 2004), and even spectral ratios (Matsuda, Tanaka, Fujita, & Iba, 2012).

To generate HS data that accurately characterizes reflectance of a target, radiometric calibration is essential to produce useful data from gantry, imaging chamber, and point-view sources (Bai et al., 2019; V. S. Ciganda & Gitelson, 2008; Condorelli et al., 2018; Martínez-Martínez, Gomez-Gil, Machado, & Pinto, 2018; Römer et al., 2012). Controlled imaging facilities aim to manage variables that influence HS data quality such as background reflectance (Elsayed, Mistele, & Schmidhalter, 2011; Kolber et al., 2005; Zarco-Tejada, Ustin, & Whiting, 2005), sensor height and angle (Crusiol et al., 2017; He et al., 2016; Herrmann et al., 2018), and shading (Corti, Marino Gallina, Cavalli, & Cabassi, 2017; Jay et al., 2017). Another approach to calibrating plant spectra is taking into account anatomy, reconstructing 3D canopies (Behmann et al., 2015; Bellasio, Olejníčková, Tesař, Šebela, & Nedbal, 2012; Biskup, Scharr, Schurr, & Rascher, 2007; Neilson et al., 2015; Paproki, Sirault, Berry, Furbank, & Fripp, 2012; Paulus, 2019; Thapa, Zhu, Walia, Yu, & Ge, 2018; Zhou et al., 2019). This focus on architecture has led to organ-level segmentation, where leveraging spatial data has effectively predicted diseases (Abdu, Mokji, & Sheikh, 2019; Nagasubramanian et al., 2019), linked geometric traits to desired heritable genes (Miao et al., 2020), and identified drought stress via leaf incident angle (Behmann et al., 2016). Spectra carry useful data that becomes more relevant when accounting for lurking environmental factors.

Currently, spectral profiles of plants collected from either top or side view cameras are averaged to a single spectral profile (Bruning et al., 2019; Herrmann et al., 2018; Pandey, Ge, Stoerger, & Schnable, 2017) (Du et al., 2016; Haboudane et al., 2004). This approach provides limited information about plant condition because it does not take into account within canopy variation in neither plant traits (Blackburn, 1998; Lemaire & Gastal, 1997; H. Li, Zhao, Yang, & Feng, 2015) nor illumination patterns (Mercado et al., 2006). Vegetative age and development stage confound the predictive power of spectral data (Elsayed et al., 2011; Fiorani, Rascher, Jahnke, & Schurr, 2012; Zarco-Tejada et al., 2005). Standardizing sampling positions for HS point-collections (V. Ciganda, Gitelson, & Schepers, 2008; Yuan et al., 2016) and designing multi-angled metrics (He et al., 2016) are strategies to mitigate the impact of non-uniform canopy spectra. Despite its potential to obfuscate HS signals of plant health and distress, the literature does not characterize variance in spectral reflectance along vertical canopy profiles, (Gara, Darvishzadeh, Skidmore, & Wang, 2018; Gara, Skidmore, Darvishzadeh, & Wang, 2019; H. Li, Zhao, Huang, & Yang, 2013; H. Li et al., 2015; Ye et al., 2018). A knowledge gap exists in that

spectral variability has not explicitly been measured between canopy positions, nor utilized to classify crop responses to environmental stresses.

The following research aimed to directly leverage HS variability within the highest five nodes of soybean plants (*Glycine Max*) to detect drought and nitrogen stress treatments. Soybean was investigated due to the species' ubiquity in contemporary agriculture, and tissue biochemical concentrations were established via High-performance liquid chromatography (HPLC) analysis of extract separations and Partial Least Squares Regression (PLSR). While prior work has scaled leaf-level data by its cumulative LAI (Gara, Skidmore, et al., 2019), in this experiment spectra are directly compared between node positions with spectral angle measurements (SAM) and percent difference between NDVI to represent commonly utilized VIs. Single NDVI values and ratios between node positions are compared in efficacy at discerning each of the treatment groups using post-hoc testing. Finally, Linear Discriminant Analysis (LDA) classifiers built on relative reflectance between node positions are compared against analogous models built on point-view spectra.

2. MATERIALS AND METHODS

2.1 Experimental Design

In 14-1 of the Lily Hall of Life Sciences Greenhouse at Purdue University, dry-down and nitrogen deprivation treatments were executed in a factorial experimental design in replicates of 12. Williams 82 soybean plants (*Glycine Max*) were grown in randomized block without Rhizobium inoculation in Berger soilless media (coarse sphagnum peat moss (70-75%), perlite, composted sphagnum peat moss, and vermiculite). Control samples were watered to saturation with one liter of nutrient solution every four days, and on the data collection day. Fertilization was delivered with ICL 20N-1.3P-15.8K Specialty Fertilizers solution using reverse osmosis water at a concentration of 150 N, 9.8 P, 119 K, 12 Mg, 21 S, 1.5 Fe, 0.4 Mn and Zn, 0.2 Cu and B, and 0.1 Mo mg/L, with 61% nitrate and 39% ammoniacal sources. Using 0.734 gallon pots with a diameter of 16.2 cm, this fertilization is equivalent to 72.8 kg N/hectare and 36.4 kg N/hectare respectively for control and nitrogen-deprived treatments.

Dry-down lasted for 10 or 11 days, beginning when most of the plants were at V5 maturity. Visual inspection monitored for pests, which did not emerge over the experiment. Greenhouse temperature maintained within 23.9-32.2°C over the 32 days growing period extending from planting on October 6th, 2019 to the data collection days on November 7th and 8th 2019. Five equally spaced 500W halogen lamps supplemented lighting from 6:00am to 8:00pm.

2.2 HS Measurements

A Spectra Vista Corporation (SVC) HR-1024 spectroradiometer captured samples' point measurements. Using a leaf clip, two spectra were collected from the center trifoliate at the highest five nodes per plant to be averaged together, resulting in 235 point-view spectra. White references were taken every six samples. The sensor has spectral resolution from 350 nm to 2500 nm with respective intervals of 1.5 nm, 3.8 nm, and 2.5 nm for the 350-1000 nm, 1000-1890 nm, and 1890-2500 nm regions. Spectra were interpolated into 1.0 nm steps. NDVI was computed for each point-sampling position as $(R_{800} - R_{650})/(R_{800} + R_{650})$. Analysis was limited to the first trifoliate leaves from Nodes 1-4 from the top, excluding the highest due to challenging sampling logistics and

higher noise. Within each plant, SAMs were computed exhaustively between node position spectra as in Kruse et al. 1993. Spectral angle between spectrum can by calculated with the following formula, where y and r are sources with reflectance values in bands from i to n:

$$\alpha = \cos^{-1} \frac{\sum_{i=1}^{n} y_i r_i}{\sqrt{\sum_{i=1}^{n} y_i^2} \sqrt{\sum_{i=1}^{n} r_i^2}}$$

Each datum was labeled based on the source leaflet's position from the highest node of the plant, inspired by the Lindenmayer naming convention (Prusinkiewicz, 1998). This system is suited to soybean's anatomical plasticity and applicable to indeterminate, determinate, and semi-determinate varieties.

2.3 Reference Measurements

Determining total nitrogen content and the concentrations (mg/g DW) of neoxanthin, violaxanthin, lutein, zeaxanthin, chlorophyll a&b, and B-carotene in tissue samples validated the effects of the nitrogen deprivation and drought stress. For N and pigment concentrations, 118 and 116 tissues were processed for concentrations, respectively. This set of samples represented each node position and treatment combination. Referenced leaves were then used to generate a PLSR models per chemical to predict the concentrations of the rest of the spectral measurements.

Standard analytical determination of foliar carbon and nitrogen was performed using a Thermo Finnigan Flash 1112 elemental analyzer (San Jose, CA, USA). Pigments were quantified via HPLC following Cotrozzi et al (2016). Briefly, 50mg of lyophilized leaf material was homogenized with 1mL HPLC-grade methanol in a 2mL microtube. After incubating overnight at 4°C in darkness, samples were centrifuged for 15 min at 15,000 rpm. Supernatant was filtered through a 0.2 um Ministart SRT15 aseptic filter into amber HPLC vials for assessment and then run on a Shimadzu Prominence HPLC system with a PDA detector. Pigments were eluted with a solvent of 75% acetonitrile, 25% methanol for 14 minutes followed by a 1.5 linear gradient to a solvent of 68% methanol, 32% ethylacetate. The second solvent ran for another 14.5 minutes followed by a 2-minute linear gradient back to the first solvent for 5 minutes to equilibrate the

column. The flow rate was 1 mL/min with an injection volume of 25 µL, and pigments were identified based on their absorbance at 445 nm compared to pure standards.

Finally, the dry-down treatment was validated by deriving relative water content (RWC) per plant from tissue collected from the third highest node. This investigation acknowledges that these greenhouse results will not be directly transferrable to field hyperspectral data nor modern germplasm lines. Etiolation observed in samples may have affected spectral and chemical trends.

2.4 Statistical Tests

Matlab R2019a and The Field Spectroscopy Facility (FSF) Post Processing Toolbox imported, referenced, and delivered the spectroradiometer data. Python 3.6 *scipy*, *sklearn*, and *matplotlib* generated all visualizations and statistical analysis. The following methods and tests served to support the validation and evaluation of the experiment and its findings. Alpha was set to 0.05 and bootstrapping for mean values was set to 1000 resamples for 95% confidence intervals.

2.4.1 Referencing Tissue Photopigment and Nitrogen Concentrations

Photopigment concentrations were required for each imaged location in order to evaluate the significance of their relationships with treatment and node height. For chemical concentration, PLSR models built on established extracts and their spectra predicted the concentrations from the spectra of unreferenced samples (Wold, Ruhe, Wold, & Dunn, 1984; Wold, Sjostrom, & Eriksson, 2001). PLSR reduces the highly-dimensional spectra into latent variables which best predict the dependent pigment concentrations (Wegelin, 2000). Each model was refined using nested cross-validation (20 repetitions each) to tune to the optimal number of latent variables and generate train/test explained variance and root mean squared error (RMSE).

2.4.2 Quantify Significant Biochemical between Nodes and Treatments

Welch's ANOVA was used to test whether tissue concentrations were uniform across node heights or treatment groups. This test compares the means of groups, and is used on balanced, approximately normal data with heterogeneous variance between groups.

2.4.3 Evaluate Spectral Variability Pairwise Comparisons with Concentrations and VI Data with respect to Node Position and Treatment

Across treatments and node positions, a 3-way ANOVA tested the uniformity of NDVI intensities. When evaluating with respect to only treatment or node position, NDVI and NDVI ratios were evaluated with Welch's ANOVA. Following a rejected null hypothesis from a Welch's ANOVA test, post-hoc Tamhane's T2 tests identified which pairwise comparisons were significantly different between canopy positions or between treatment groups. Tamhane's T2 test conservatively evaluates data that is approximately normal with different variance between compared groups.

2.4.4 Classify Treatments based on Point Spectra or Relative Reflectance Spectra

Multiclass LDA models were trained on either spectra point-measurements or relative reflectance between various node positions, which emphasized intra-canopy spectral variability. These nonparametric classifiers performed dimensionality reduction on the spectra via singular value decomposition to maximize the distance between treatment groups in a projected linear subspace (Hastie, Tibshirani, & Friedman, 2008). Each classifier was refined using nested cross-validation (20 repetitions each) to tune based on F1-score and track precision, recall, accuracy, and kappa performance metrics. Confusion matrices summarized the classification performance across the treatments.

3. VALIDATION

3.1 Biochemical Concentrations over Node Positions

Chemical and RWC referencing characterized 47 plants (one sample died before data collection) to validate the impacts of the nitrogen-deprivation and dry-down treatments. While RWC was collected for each plant, PLSR completed the full set of photopigment and nitrogen concentrations with the unreferenced positions' spectra.

Nonparametric tests were used because homogeneity of variance was violated. Normal QQ plots deemed each concentration dataset acceptably normal, though each concentration and RWC with respect to treatment rejected homogeneous variance with $p = 1.1e4$ and $p = 3.7e4$ respectively from Levene's Test.

Table 1 summarizes the performance of the optimized chemical concentration PLSR models. Modeling ChlA/ChlB generated high RMSE (test = 1.43 +/- 1.45) with only 0.03 +/- 0.10 explained variance. To contrast, the model for nitrogen percent is comparable to the work of Bruning et. al (2019) who regressed using top-view HS data (400-2500 nm) to get validation R2 and RMSE scores of 0.60 and 0.43 respectively.

Table 1: PLSR Train and Test Cross Validation Performance Metrics

Metric	Neoxanthin (mg/g DW)	Violaxanthin (mg/g DW)	Lutein (mg/g DW)	Zeaxanthin (mg/g DW)	Chlorophyll a+b (mg/g DW)	Chlorophyll a/Chlorophyll b	B-carotene (mg/g DW)	Nitrogen (%)
NLV	4	3	3	5	4	2	3	16
Train Explained Var.	0.67 (+/- 0.07)	0.42 (+/- 0.06)	0.65 (+/- 0.07)	0.75 (+/- 0.10)	0.57 (+/- 0.10)	0.10 (+/- 0.04)	0.42 (+/- 0.09)	0.96 (+/- 0.02)
Test Explained Var.	0.55 (+/- 0.37)	0.25 (+/- 0.25)	0.57 (+/- 0.25)	0.31 (+/- 1.18)	0.46 (+/- 0.28)	0.03 (+/- 0.10)	0.44 (+/- 0.26)	0.20 (+/- 2.90)
Train RMSE	0.03 (+/- 0.01)	0.02 (+/- 0.01)	0.20 (+/- 0.07)	0.01 (+/- 0.01)	2.29 (+/- 0.86)	1.45 (+/- 0.95)	0.71 (+/- 0.29)	0.17 (+/- 0.10)
Test RMSE	0.03 (+/- 0.02)	0.02 (+/- 0.01)	0.22 (+/- 0.13)	0.01 (+/- 0.01)	2.48 (+/- 1.49)	1.43 (+/- 1.45)	0.67 (+/- 0.48)	0.80 (+/- 1.59)

NLV is Number of Latent Variables

The complete chemical concentrations dataset is displayed in Figure 1. When evaluated within treatments and along nodes with Welch's ANOVA, concentrations are significantly non-uniform for except for nitrogen percent in irrigated groups, B-carotene in the drought-stress treatment, and zeaxanthin in any of the treatment groups. B-carotene concentrations may have increased in the drought conditions due to accumulation in tissues due to stunting. When evaluating with Welch's ANOVA at each node position, the only concentrations which did not vary with respect to treatment were neoxanthin at nodes 3 and 4 as well as ChlA/ChlB at node 2. The ChlA/ChlB model's weak performance precluded researchers to not rely on its predictions.
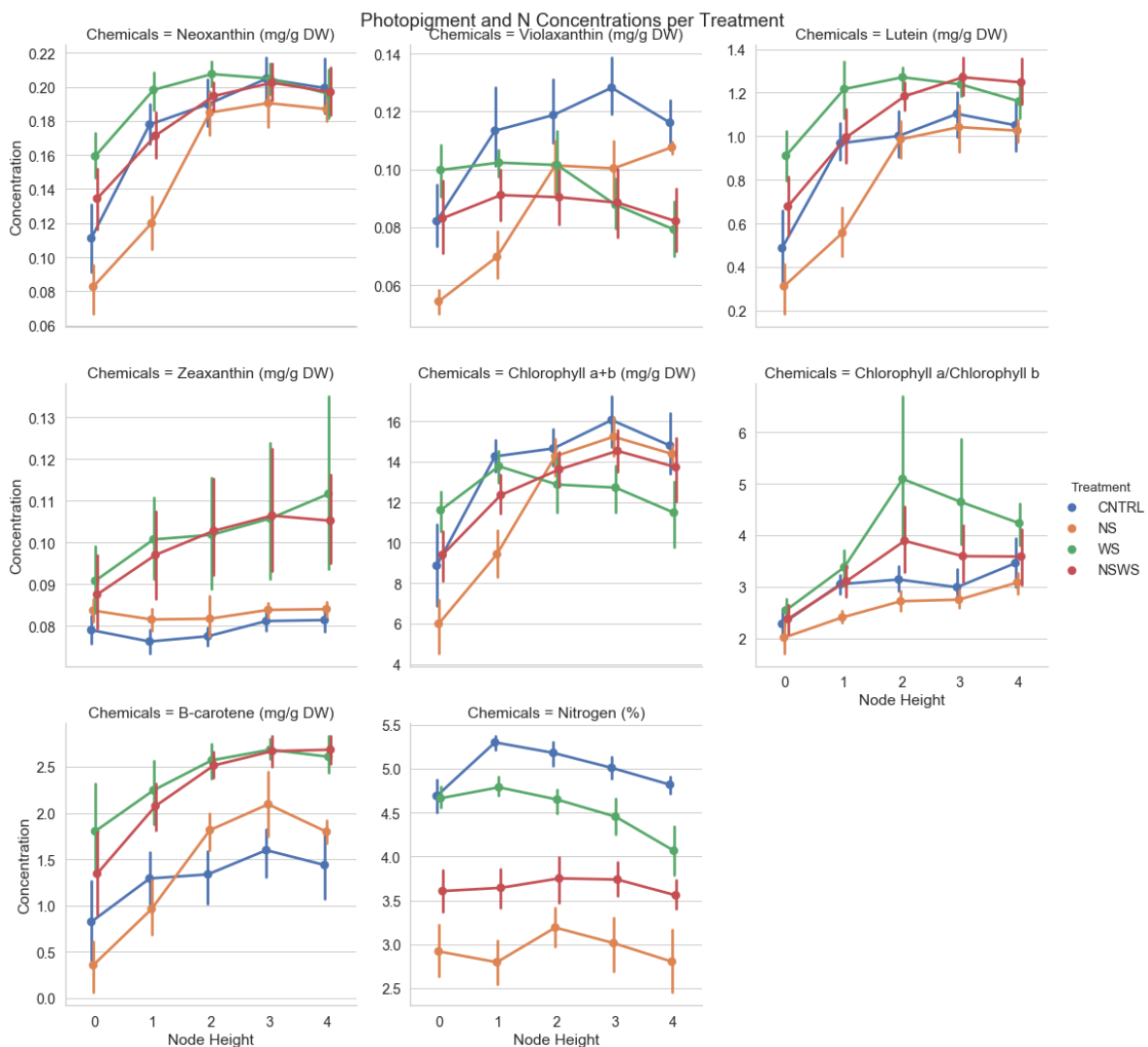
Figure 1: PLSR generated photopigment and nitrogen concentrations were generally significantly non-uniform per treatment and node positions according to Welch's ANOVA. Reduced nitrogen (%) and total Chl validate the nitrogen stress, while elevated zeaxanthin, and lutein validated the drought-stress.

Along analogous tissues subjected to the nitrogen-stress, overall chlorophyll concentration and percent nitrogen were reduced. This behavior validated the nitrogen deprivation, as it is typical of nutrient deprivation (Fang, Bouwkamp, & Solomos, 1998; Liu et al., 2009). Furthermore, nitrogen's apparent non-uniform descending trend is supported in the literature, where vertical nitrogen concentrations are tied to LAI (Grindlay, 1997; Hirose & Werger, 1987; Lemaire & Gastal, 1997; Pons, Schieving, Hirose, & Werger, 1990; Shiraiwa & Sinclair, 1993)

As displayed in Figure 2, RWC was significantly different between the irrigated and drought-treated groups. Water-stress was further validated in the significant increase in concentration of xanthophyll pigments zeaxanthin and lutein with respect to control as protections against oxidative stress (Altangerel et al., 2017; Havaux, 1998; Jaleel et al., 2009).

Significantly distinct by Welch's ANOVA
Significantly unique by Tamhane T2's Test
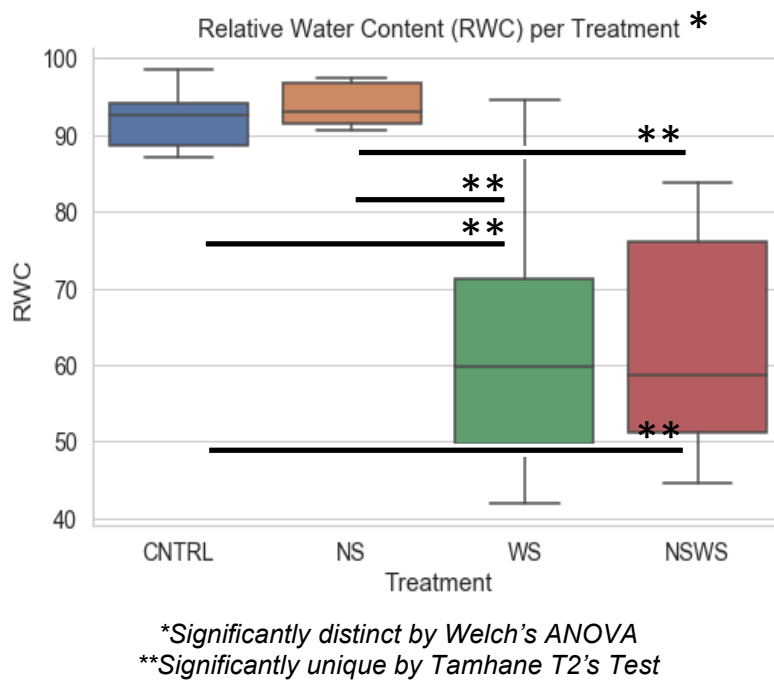
Figure 2: RWC per treatment was visibly and significantly distinct. Each treatment's RWC was respectively significantly indistinguishable and distinct from their shared and opposed irrigation regimens.

4. RESULTS AND DISCUSSION

4.1 Spectral variability across node positions

SAMs were generally greater between nodes that were further apart, but treatment-specific responses appeared in the magnitudes. Across intra-canopy comparisons shown in Figure 3, drought-stressed spectra vary less between node positions than in the other treatments, even at the most extreme pairings where the data is more variable (this is explicitly presented in Table 2).

*Significantly distinct by Welch's ANOVA
**Significantly unique by Tamhane T2's Test
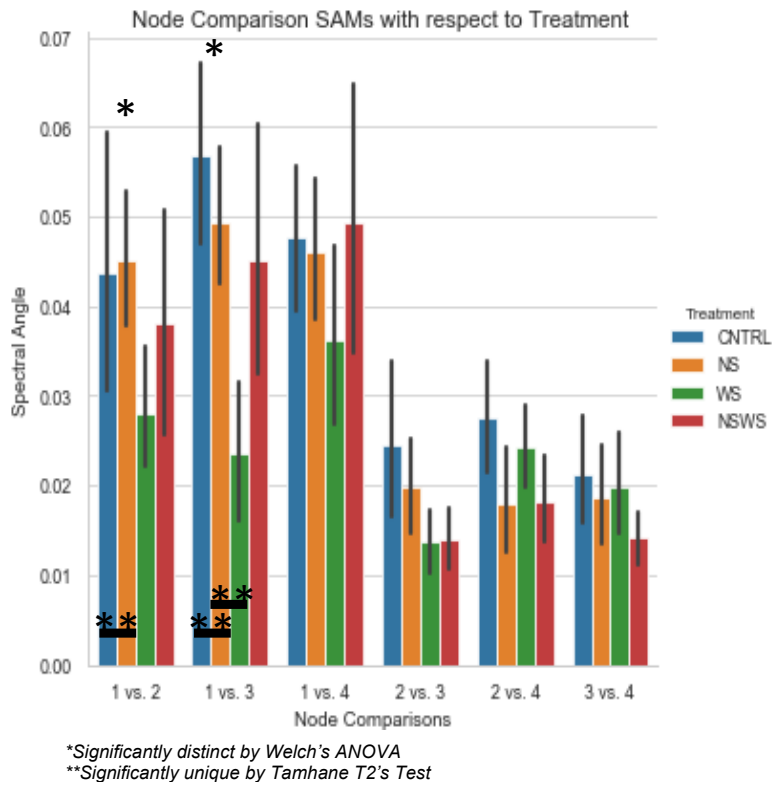
Figure 3: Spectral divergence between nodes of greater relative age difference or distance trends to be greater. These magnitudes, however, are significantly influenced by treatment when comparing nodes 1 vs. 2 and nodes 1 vs. 3.

Table 2: Mean SAM and Standard Deviation between Node Positions per Treatment

Node Comparison	CNTRL	NS	NSWS	WS
1 vs. 2	0.044, 0.025	0.045, 0.013	0.038, 0.024	0.028, 0.011
1 vs. 3	0.057, 0.018	0.049, 0.014	0.045, 0.026	0.024, 0.014
1 vs. 4	0.048, 0.014	0.046, 0.015	0.049, 0.028	0.036, 0.018
2 vs. 3	0.025, 0.015	0.020, 0.009	0.014, 0.006	0.014, 0.006
2 vs. 4	0.028, 0.012	0.018, 0.010	0.018, 0.009	0.024, 0.009
3 vs. 4	0.021, 0.011	0.019, 0.010	0.014, 0.005	0.020, 0.011

Node position's influence on SAM magnitude could be partially explained by tissues' relative maturities, as developing mesophilic tissue influences the path and absorption of light, fundamentally shifting vegetation's reflectance (Rapaport, Hochberg, Rachmilevitch, & Karnieli, 2014). Leaf age has been shown to influence abiotic and biotic stress responses, which inform HS data collection methods (Berens et al., 2019; Elvanidi, Katsoulas, & Kittas, 2018). Additionally, the dynamics of photosynthesis with respect to younger, more intensely illuminated tissues compared to those with more diffuse illumination could also be culpable (Gara, Darvishzadeh, Skidmore, Wang, & Heurich, 2019; Mercado et al., 2006). To model canopy compositions, sensor positioning balances the need to capture representative canopy data (Elvanidi et al., 2018; Ye et al., 2018) with maintaining signal over noise (Martínez-Martínez et al., 2018).

4.2 Efficacies of intra-canopy combination VIs at distinguishing abiotic distress treatments

SAM reports the magnitude of spectral variability, but without specifying which chemometrically relevant wavelengths are responsible. As an illustrative example of potential VI non-uniformity, NDVI was plotted with respect to treatment and node position, displayed in Figure 4A. Results from a 3-way ANOVA evaluated the relationship of watering, fertilizing, and node position as features with respect to NDVI in Table 3. Water treatment and node height were significant factors individually, though the nitrogen treatment was significant in its interaction with irrigation or with irrigation and node height. With these findings, NDVI does not appear equally sensitive to water and nitrogen stresses.

Table 3: Node height, nitrogen treatment, and water treatment relationships with NDVI intensity

Feature	Sum of Squares	DoF	F	P-value
Intercept	8.111	1	21648.68	**7.91e-183**
C(Water)	7.77e-3	1	20.731	**9.97e-6**
C(Nitrogen)	2.43e-4	1	0.649	0.422
C(Node Height)	0.010	3	9.303	**9.83e-6**
C(Water):C(Nitrogen)	3.86e-3	1	10.300	**1.59e-3**
C(Water):C(Node Height)	0.022	3	19.929	**3.91e-11**
C(Nitrogen):C(Node Height)	2.66e-4	3	0.237	0.871
C(Water):C(Nitrogen):C(Node Height)	3.58e-3	3	3.183	**0.025**

Within each treatment group, post-hoc analysis after a failed Welch's ANOVA reveal significant variability at specific node comparisons (Figure 4B). In stressed treatments, comparisons between the highest and lowest tissues were significant, and the greatest proportion of significant NDVI node comparisons came from the nitrogen-stressed samples. The directionality of NDVI changes between nodes in nitrogen-stressed samples were mirrored in the control, but the magnitude made the stress response distinct. Water-stressed treatments shared a characteristic NDVI decline in from the highest to lowest canopy positions.
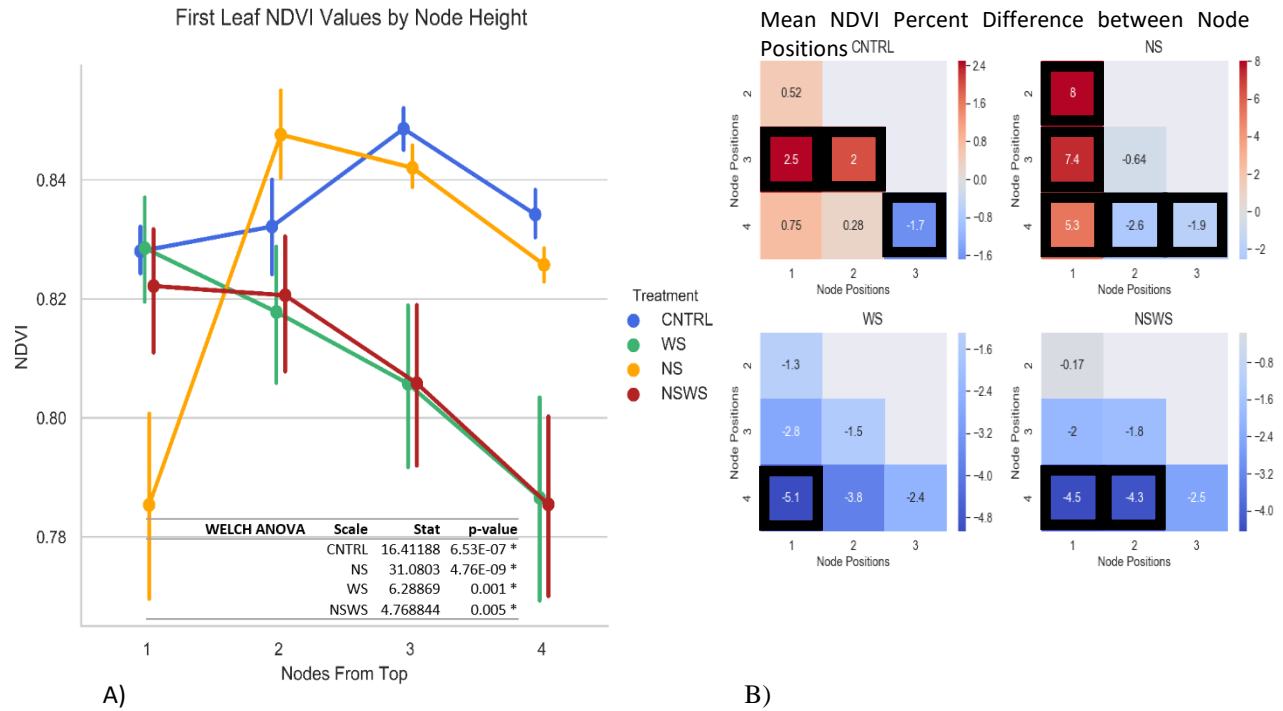
Figure 4: Nonlinear trends appear in NDVI intensity along node positions, which include changes in rank between treatments depending on node height. Error bars are 95% CI (A). Significant changes in NDVI intensity between node positions characterize sample responses to drought and nitrogen stresses via magnitude and directionality of the changes (B).

Nitrogen-stress is likely so apparent in post-hoc testing due to NDVI's constituent wavelengths NIR and red being stronger correlated to key nitrogen-incorporating pigments than to a direct water absorption feature (Peñuelas, Josep; Filella & Gamon, 1995).

The significant NDVI fluctuations within canopy were tested as a signal to separate treatment groups with additional post-hoc testing. Single and ratios of NDVI readings distinguished between the treatments to variable efficacy, summarized in Figure 5. The only NDVI point-measurement effective at differentiating all treatments was at the fifth node from the top (node 4). Alternatively, ratio NDVI metrics were also effective (Node 1 vs. Node 3, Node 1 vs. Node 4) and to greater statistical significance.
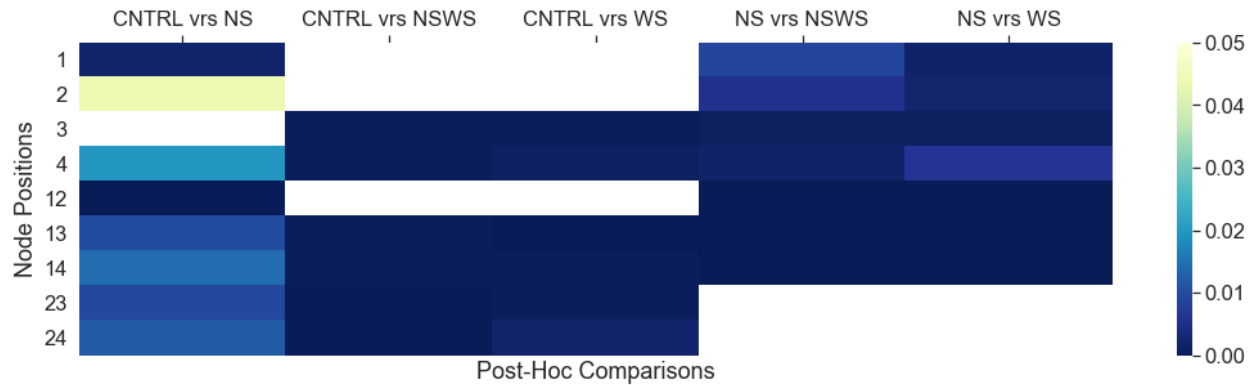
Figure 5: Post-Hoc significance of NDVI at discerning between treatments as single measurements or ratios between node positions. Point-view NDVI and combination NDVI metrics can significantly discern between all of the treatments, though the ratio metrics do so to greater statistical significance.

These results indicate that the variability in NDVI intensity between canopy positions can be more effective at discerning treatment groups than point measurements. Individual locations can be effective, but the lurking effects of canopy position are observed in the literature. Even when controlling sampling positions for collecting point view data, it is possible vegetative maturation can influence the collected spectra in addition to environmental stresses (Herrmann et al., 2018; Rapaport et al., 2014; Yuan et al., 2016)

1.3 LDA Classification using single-measurements spectra or relative reflectance between positions

Built on individual spectra or ratios between pairs of positions, multiclass LDA models were tuned using nested cross-validation (repeats=20) with an external cross-validation, selecting for F1-Score. The performance metrics from outer CV with their 95% confidence intervals are summarized in Table 4, where classifiers built on data from Node 1, Node 3, or their ratio performed superiorly.

Table 4: LDA Performance metrics with 95% CI: Overall and per Treatment

Node Data	Precision	Recall	F1-Score	Accuracy	Kappa
1 vs. 3	**0.83 (+/- 0.22)**	**0.83 (+/- 0.22)**	**0.81 (+/- 0.23)**	**0.82 (+/- 0.21)**	**0.75 (+/- 0.21)**
1	0.82 (+/- 0.15)	0.81 (+/- 0.17)	0.79 (+/- 0.19)	0.80 (+/- 0.21)	0.73 (+/- 0.21)
3	0.78 (+/- 0.30)	0.80 (+/- 0.27)	0.76 (+/- 0.29)	0.77 (+/- 0.26)	0.69 (+/- 0.26)
1 vs. 4	0.71 (+/- 0.23)	0.70 (+/- 0.22)	0.67 (+/- 0.20)	0.72 (+/- 0.19)	0.61 (+/- 0.19)
2	0.70 (+/- 0.21)	0.71 (+/- 0.13)	0.66 (+/- 0.18)	0.68 (+/- 0.17)	0.57 (+/- 0.17)
1 vs. 2	0.66 (+/- 0.19)	0.64 (+/- 0.24)	0.61 (+/- 0.20)	0.64 (+/- 0.16)	0.51 (+/- 0.16)
4	0.64 (+/- 0.25)	0.66 (+/- 0.26)	0.61 (+/- 0.23)	0.63 (+/- 0.24)	0.51 (+/- 0.24)
2 vs. 3	0.62 (+/- 0.25)	0.59 (+/- 0.25)	0.56 (+/- 0.25)	0.61 (+/- 0.24)	0.47 (+/- 0.24)
2 vs. 4	0.54 (+/- 0.18)	0.54 (+/- 0.22)	0.50 (+/- 0.20)	0.54 (+/- 0.20)	0.38 (+/- 0.20)
3 vs. 4	0.33 (+/- 0.26)	0.32 (+/- 0.24)	0.28 (+/- 0.20)	0.30 (+/- 0.21)	0.09 (+/- 0.21)

The Node 1/Node 3 classifier performed the best overall, followed by the Node 1 classifier. In Table 5, confusion matrices for both classifiers illustrate how the Node 1 classifier was more confused in detecting the water stressed samples. While the Node 1/Node 3 classifier was less effective at identifying the nitrogen stressed samples, it had lower or comparable variability for the rest of the treatments.

Table 5: Mean Confusion Matrices and confidence intervals for classifiers built on Node 1 and Node 1/Node 3 spectra

Node 1/Node 3

	CNTRL	WS	NS	NSWS
CNTRL	**0.912 (+/- 0.234)**	0.0 (+/- 0.0)	0.065 (+/- 0.22)	0.022 (+/- 0.136)
WS	0.0 (+/- 0.0)	**0.837 (+/- 0.368)**	0.0 (+/- 0.0)	0.163 (+/- 0.368)
NS	0.056 (+/- 0.23)	0.0 (+/- 0.0)	0.909 (+/- 0.3)	0.035 (+/- 0.23)
NSWS	0.077 (+/- 0.27)	0.262 (+/- 0.472)	0.012 (+/- 0.108)	0.599 (+/- 0.578)

Node 1

	CNTRL	WS	NS	NSWS
CNTRL	0.912 (+/- 0.326)	0.012 (+/- 0.108)	0.025 (+/- 0.218)	0.05 (+/- 0.254)
WS	0.02 (+/- 0.174)	0.736 (+/- 0.502)	0.03 (+/- 0.146)	0.214 (+/- 0.472)
NS	0.0 (+/- 0.0)	0.0 (+/- 0.0)	**0.978 (+/- 0.136)**	0.022 (+/- 0.136)
NSWS	0.153 (+/- 0.494)	0.22 (+/- 0.436)	0.01 (+/- 0.088)	**0.617 (+/- 0.548)**

Figure 7 presents the ratio of spectra between Nodes 1 and 3, in which relative reflectance per treatment reveals distinctive features. By emphasizing spectral variability resulting from treatment, sampling groups were separated as in Matsuda et al. 2012. It is possible that the relative reflectance model's advantage was by capturing non-uniform hyperspectral signals in canopies (Römer et al., 2012) that could be tied to age-mediated responses to stresses (Berens et al., 2019). In the literature, the usefulness of HS data collected from canopies compared to leaf measures depends how much of the plants are in view (Herrmann et al., 2018; Martínez-Martínez et al., 2018; Mishra et al., 2017). SAMs between Nodes 1 and 3 were among the largest overall as they represent distinct portions of the canopy, though the water/nitrogen stressed samples had greater variability at this comparison. It is possible this unequal noise contributed to the relative reflectance model's confusion in classifying the water/nitrogen stressed samples compared to the Node 1 model.
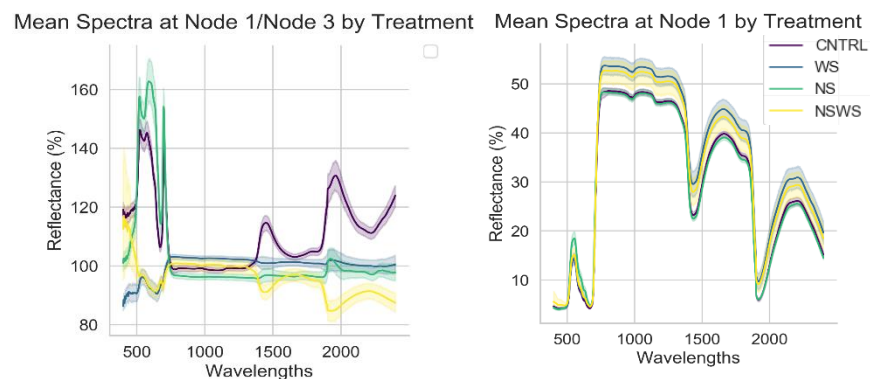

Figure 6: The transformed Node 1 vs. Node 3 spectra had distinctive shape, but overall greater variance over the range and within treatments. Node 1 data, on the other hand, had observably greater variability in the drought treatments compared to the irrigated.

5. CONCLUSIONS

As phenotyping technologies become ubiquitous in plant breeding and farming operations, it is our obligation to account for significant and known signal noise in our methods. In this project, soybeans were subjected to nitrogen and drought stress were distinguished apart by leveraging HS heterogeneity collected from the highest nodes. SAMs and percent NDVI differences between node positions quantified spectral heterogeneity with respect to treatments, and spectral stress responses displayed characteristic non-uniform, directional, and significant NDVI intensity trends. Leveraging spectral variability revealed that NDVI ratios proved more statistically effective at discerning treatments than individual leaf NDVI values and a LDA classifier built on relative reflectance delivered more uniform classification performance. This work will inform and justify the design of organ-level HS segmentation and more effective sensing methods to detect plant and canopy health statuses. Understanding the signal in canopy spectral variability is an opportunity to develop more comprehensive phenotyping tools to swiftly glean actionable information on expressed crop stresses and resiliencies.

WORKS CITED

Abdu, A. M., Mokji, M. M., & Sheikh, U. U. (2019). A Pattern Analysis-based Segmentation to Localize Early and Late Blight Disease Lesions in Digital Images of Plant Leaves. *2019 IEEE International Conference on Signal and Image Processing Applications (ICSIPA)*, 116–121. IEEE.

Altangerel, N., Ariunbold, G. O., Gorman, C., Alkahtani, M. H., Borrego, E. J., Bohlmeyer, D., … Scully, M. O. (2017). In vivo diagnostics of early abiotic plant stress response via Raman spectroscopy. *Proceedings of the National Academy of Sciences of the United States of America*, *114*(13), 3393–3396. https://doi.org/10.1073/pnas.1701328114

Bai, G., Ge, Y., Scoby, D., Leavitt, B., Stoerger, V., Kirchgessner, N., … Awada, T. (2019). NU-Spidercam: A large-scale, cable-driven, integrated sensing and robotic system for advanced phenotyping, remote sensing, and agronomic research. *Computers and Electronics in Agriculture*, *160*(January), 71–81. https://doi.org/10.1016/j.compag.2019.03.009

Behmann, J., Mahlein, A. K., Paulus, S., Dupuis, J., Kuhlmann, H., Oerke, E. C., & Plümer, L. (2016). Generation and application of hyperspectral 3D plant models: methods and challenges. *Machine Vision and Applications*, *27*(5), 611–624. https://doi.org/10.1007/s00138-015-0716-8

Behmann, J., Mahlein, A. K., Paulus, S., Kuhlmann, H., Oerke, E. C., & Plümer, L. (2015). Calibration of hyperspectral close-range pushbroom cameras for plant phenotyping. *ISPRS Journal of Photogrammetry and Remote Sensing*, *106*, 172–182. https://doi.org/10.1016/j.isprsjprs.2015.05.010

Bellasio, C., Olejníčková, J., Tesař, R., Šebela, D., & Nedbal, L. (2012). Computer reconstruction of plant growth and chlorophyll fluorescence emission in three spatial dimensions. *Sensors*, *12*(1), 1052–1071. https://doi.org/10.3390/s120101052

Berens, M. L., Wolinska, K. W., Spaepen, S., Ziegler, J., Nobori, T., Nair, A., … Tsuda, K. (2019). Balancing trade-offs between biotic and abiotic stress responses through leaf age-dependent variation in stress hormone cross-talk. *Proceedings of the National Academy of Sciences of the United States of America*, *116*(6), 2364–2373. https://doi.org/10.1073/pnas.1817233116

Biskup, B., Scharr, H., Schurr, U., & Rascher, U. (2007). A stereo imaging system for measuring structural parameters of plant canopies. *Plant, Cell and Environment*, *30*(10), 1299–1308. https://doi.org/10.1111/j.1365-3040.2007.01702.x

Blackburn, G. A. (1998). Quantifying chlorophylls and carotenoids at leaf and canopy scales: An evaluation of some hyperspectral approaches. *Remote Sensing of Environment*, *66*(3), 273–285. https://doi.org/10.1016/S0034-4257(98)00059-5

Blackburn, G. A. (2007). Hyperspectral remote sensing of plant pigments. *Journal of Experimental Botany*, *58*(4), 855–867. https://doi.org/10.1093/jxb/erl123

Bruning, B., Liu, H., Brien, C., Berger, B., Lewis, M., & Garnett, T. (2019). The Development of Hyperspectral Distribution Maps to Predict the Content and Distribution of Nitrogen and Water in Wheat (Triticum aestivum). *Frontiers in Plant Science*, *10*(October), 1–16. https://doi.org/10.3389/fpls.2019.01380

Ciganda, V., Gitelson, A., & Schepers, J. (2008). Vertical profile and temporal variation of chlorophyll in maize canopy: Quantitative "crop vigor" indicator by means of reflectance-based techniques. *Agronomy Journal*, *100*(5), 1409–1417. https://doi.org/10.2134/agronj2007.0322

Condorelli, G. E., Maccaferri, M., Newcomb, M., Andrade-Sanchez, P., White, J. W., French, A. N., … Tuberosa, R. (2018). Comparative aerial and ground based high throughput phenotyping for the genetic dissection of NDVI as a proxy for drought adaptive traits in durum wheat. *Frontiers in Plant Science*, *9*(June), 1–17. https://doi.org/10.3389/fpls.2018.00893

Corti, M., Marino Gallina, P., Cavalli, D., & Cabassi, G. (2017). Hyperspectral imaging of spinach canopy under combined water and nitrogen stress to estimate biomass, water, and nitrogen content. *Biosystems Engineering*, *158*, 38–50. https://doi.org/10.1016/j.biosystemseng.2017.03.006

Crusiol, L. G. T., Carvalho, J. de F. C., Sibaldelli, R. N. R., Neiverth, W., do Rio, A., Ferreira, L. C., … Farias, J. R. B. (2017). NDVI variation according to the time of measurement, sampling size, positioning of sensor and water regime in different soybean cultivars. *Precision Agriculture*, *18*(4), 470–490. https://doi.org/10.1007/s11119-016-9465-6

Curran, P. J., Dungan, J. L., & Peterson, D. L. (2001). Estimating the foliar biochemical concentration of leaves with reflectance spectrometry: Testing the Kokaly and Clark methodologies. *Remote Sensing of Environment*, *76*(3), 349–359. https://doi.org/10.1016/S0034-4257(01)00182-1

DESA, U. (2019). Growing at a slower pace, world population is expected to reach 9.7 billion in 2050 and could peak at nearly 11 billion around 2100 | UN DESA Department of Economic and Social Affairs. Retrieved from https://www.un.org/development/desa/en/news/population/world-population-prospects-2019.html

Du, L., Gong, W., Shi, S., Yang, J., Sun, J., Zhu, B., & Song, S. (2016). Estimation of rice leaf nitrogen contents based on hyperspectral LIDAR. *International Journal of Applied Earth Observation and Geoinformation*, *44*, 136–143. https://doi.org/10.1016/j.jag.2015.08.008

Elsayed, S., Mistele, B., & Schmidhalter, U. (2011). Can changes in leaf water potential be assessed spectrally? *Functional Plant Biology*, *38*(6), 523–533. https://doi.org/10.1071/FP11021

Elvanidi, A., Katsoulas, N., & Kittas, C. (2018). Automation for water and nitrogen deficit stress detection in soilless tomato crops based on spectral indices. *Horticulturae*, *4*(4). https://doi.org/10.3390/horticulturae4040047

Fahlgren, N., Gehan, M. A., & Baxter, I. (2015). Lights, camera, action: High-throughput plant phenotyping is ready for a close-up. *Current Opinion in Plant Biology*. https://doi.org/10.1016/j.pbi.2015.02.006

Fang, Z., Bouwkamp, J. C., & Solomos, T. (1998). Chlorophyllase activities and chlorophyll degradation during leaf senescence in non-yellowing mutant and wild type of phaseolus vulgaris L. *Journal of Experimental Botany*, *49*(320), 503–510. https://doi.org/10.1093/jxb/49.320.503

Fiorani, F., Rascher, U., Jahnke, S., & Schurr, U. (2012). Imaging plants dynamics in heterogenic environments. *Current Opinion in Biotechnology*, *23*(2), 227–235. https://doi.org/10.1016/j.copbio.2011.12.010

Fiorani, F., & Schurr, U. (2013). Future Scenarios for Plant Phenotyping. *Annual Review of Plant Biology*, *64*(1), 267–291. https://doi.org/10.1146/annurev-arplant-050312-120137

Fischer, R. A., Rees, D., Sayre, K. D., Lu, Z. M., Condon, A. G., & Larque Saavedra, A. (1998). Wheat yield progress associated with higher stomatal conductance and photosynthetic rate, and cooler canopies. *Crop Science*, *38*(6), 1467–1475. https://doi.org/10.2135/cropsci1998.0011183X003800060011x

Furbank, R. T., & Tester, M. (2011). Phenomics – technologies to relieve the phenotyping bottleneck. *Trends in Plant Science*, *16*(12), 635–644. https://doi.org/10.1016/J.TPLANTS.2011.09.005

Gamon, J. A., & Surfus, J. S. (1999). Assessing leaf pigment content and activity with a reflectometer. *New Phytologist*, *143*(1), 105–117. https://doi.org/10.1046/j.1469-8137.1999.00424.x

Gao, B. (1996). NDWI—A normalized difference water index for remote sensing of vegetation liquid water from space. *Remote Sensing of Environment*, *58*(3), 257–266. https://doi.org/10.1016/S0034-4257(96)00067-3

Gara, T. W., Darvishzadeh, R., Skidmore, A. K., & Wang, T. (2018). Impact of vertical canopy position on leaf spectral properties and traits across multiple species. *Remote Sensing*, *10*(2), 1–17. https://doi.org/10.3390/rs10020346

Gara, T. W., Darvishzadeh, R., Skidmore, A. K., Wang, T., & Heurich, M. (2019). Evaluating the performance of PROSPECT in the retrieval of leaf traits across canopy throughout the growing season. *International Journal of Applied Earth Observation and Geoinformation*, *83*(July), 101919. https://doi.org/10.1016/j.jag.2019.101919

Gara, T. W., Skidmore, A. K., Darvishzadeh, R., & Wang, T. (2019). Leaf to canopy upscaling approach affects the estimation of canopy traits. *GIScience and Remote Sensing*, *56*(4), 554–575. https://doi.org/10.1080/15481603.2018.1540170

Green, R. O., Eastwood, M. L., Sarture, C. M., Chrien, T. G., Aronsson, M., Chippendale, B. J., … Williams, O. (1998). Imaging Spectroscopy and the Airborne Visible/Infrared Imaging Spectrometer (AVIRIS). *Remote Sensing of Environment*, *65*(3), 227–248. https://doi.org/10.1016/S0034-4257(98)00064-9

Grindlay, D. J. C. (1997). Towards an explanation of crop nitrogen demand based on the optimization of leaf nitrogen per unit leaf area. *Journal of Agricultural Science*, *128*(4), 377–396. https://doi.org/10.1017/S0021859697004310

Haboudane, D., Miller, J. R., Pattey, E., Zarco-Tejada, P. J., & Strachan, I. B. (2004). Hyperspectral vegetation indices and novel algorithms for predicting green LAI of crop canopies: Modeling and validation in the context of precision agriculture. *Remote Sensing of Environment*, *90*(3), 337–352. https://doi.org/10.1016/j.rse.2003.12.013

Hastie, T., Tibshirani, R., & Friedman, J. (2008). The Elements of Statistical Learning. In *Section 4.3* (pp. 106–119).

Havaux, M. (1998). Carotenoids as membrane stabilizers in chloroplasts. *Trends in Plant Science*, *3*(4), 147–151. https://doi.org/10.1016/S1360-1385(98)01200-X

He, L., Zhang, H. Y., Zhang, Y. S., Song, X., Feng, W., Kang, G. Z., … Guo, T. C. (2016). Estimating canopy leaf nitrogen concentration in winter wheat based on multi-angular hyperspectral remote sensing. *European Journal of Agronomy*, *73*, 170–185. https://doi.org/10.1016/j.eja.2015.11.017

Herrmann, I., Vosberg, S. K., Ravindran, P., Singh, A., Chang, H. X., Chilvers, M. I., … Townsend, P. A. (2018). Leaf and canopy level detection of Fusarium virguliforme (sudden death syndrome) in soybean. *Remote Sensing*, *10*(3), 1–19. https://doi.org/10.3390/rs10030426

Hirose, T., & Werger, M. J. A. (1987). Maximizing daily canopy photosynthesis with respect to the leaf nitrogen allocation pattern in the canopy. *Oecologia*, *72*(4), 520–526. https://doi.org/10.1007/BF00378977

Jaleel, C. A., Manivannan, P., Wahid, A., Farooq, M., Al-Juburi, H. J., Somasundaram, R., & Panneerselvam, R. (2009). Drought stress in plants: A review on morphological characteristics and pigments composition. *International Journal of Agriculture and Biology*, *11*(1), 100–105.

Jay, S., Gorretta, N., Morel, J., Maupas, F., Bendoula, R., Rabatel, G., … Baret, F. (2017). Estimating leaf chlorophyll content in sugar beet canopies using millimeter- to centimeter-scale reflectance imagery. *Remote Sensing of Environment*, *198*(September), 173–186. https://doi.org/10.1016/j.rse.2017.06.008

Kokaly, R. F., Asner, G. P., Ollinger, S. V., Martin, M. E., & Wessman, C. A. (2009). Characterizing canopy biochemistry from imaging spectroscopy and its application to ecosystem studies. *Remote Sensing of Environment*, *113*(SUPPL. 1), S78–S91. https://doi.org/10.1016/j.rse.2008.10.018

Kolber, Z., Klimov, D., Ananyev, G., Rascher, U., Berry, J., & Osmond, B. (2005). Measuring photosynthetic parameters at a distance: laser induced fluorescence transient (LIFT) method for remote measurements of photosynthesis in terrestrial vegetation. *Photosynthesis Research*, *84*, 121–129. https://doi.org/10.1002/1521-4052(200108)32:8<665::aid-mawe665>3.3.co;2-o

Kruse, F. A., Lefkoff, A. B., Boardman, J. W., Heidebrecht, K. B., Shapiro, A. T., Barloon, P. J., & Goetz, A. F. H. (2008). *The spectral image processing system (SIPS)-interactive visualization and analysis of imaging spectrometer data*. *163*(January 1992), 192–201. https://doi.org/10.1063/1.44433

Le Maire, G., François, C., & Dufrêne, E. (2004). Towards universal broad leaf chlorophyll indices using PROSPECT simulated database and hyperspectral reflectance measurements. *Remote Sensing of Environment*, *89*(1), 1–28. https://doi.org/10.1016/j.rse.2003.09.004

Lemaire, G., & Gastal, F. (1997). N Uptake and Distribution in Plant Canopies. *Diagnosis of the Nitrogen Status in Crops*, *53*(370), 3–43. https://doi.org/10.1007/978-3-642-60684-7_1

Li, H., Zhao, C., Huang, W., & Yang, G. (2013). Non-uniform vertical nitrogen distribution within plant canopy and its estimation by remote sensing: A review. *Field Crops Research*, *142*(11), 75–84. https://doi.org/10.1016/j.fcr.2012.11.017

Li, H., Zhao, C., Yang, G., & Feng, H. (2015). Variations in crop variables within wheat canopies and responses of canopy spectral characteristics and derived vegetation indices to different vertical leaf layers and spikes. *Remote Sensing of Environment*, *169*, 358–374. https://doi.org/10.1016/j.rse.2015.08.021

Li, L., Zhang, Q., & Huang, D. (2014). A review of imaging techniques for plant phenotyping. *Sensors (Switzerland)*, *14*(11), 20078–20111. https://doi.org/10.3390/s141120078

Liu, N., Lin, Z. F., Van Devender, A., Lin, G. Z., Peng, C. L., Pan, X. P., … Gu, Q. (2009). Spectral reflectance indices and pigment functions during leaf ontogenesis in six subtropical landscape plants. *Plant Growth Regulation*, *58*(1), 73–84. https://doi.org/10.1007/s10725-008-9353-9

Mahlein, A.-K., Kuska, M. T., Behmann, J., Polder, G., & Walter, A. (2018). Hyperspectral

Sensors and Imaging Technologies in Phytopathology: State of the Art. *Annual Review of Phytopathology*, *56*(1), 535–558. https://doi.org/10.1146/annurev-phyto-080417-050100

Martínez-Martínez, V., Gomez-Gil, J., Machado, M. L., & Pinto, F. A. C. (2018). Leaf and canopy reflectance spectrometry applied to the estimation of angular leaf spot disease severity of common bean crops. *PLoS ONE*, *13*(4), 1–12. https://doi.org/10.1371/journal.pone.0196072

Matsuda, O., Tanaka, A., Fujita, T., & Iba, K. (2012). Hyperspectral imaging techniques for rapid identification of arabidopsis mutants with altered leaf pigment status. *Plant and Cell Physiology*, *53*(6), 1154–1170. https://doi.org/10.1093/pcp/pcs043

Mercado, L., Lloyd, J., Carswell, F., Malhi, Y., Meir, P., & Nobre, A. D. (2006). Modelling Amazonian forest eddy covariance data: A comparison of big leaf versus sun/shade models for the C-14 tower at Manaus I. Canopy photosynthesis. *Acta Amazonica*, *36*(1), 69–82. https://doi.org/10.1590/s0044-59672006000100009

Miao, C., Pages, A., Xu, Z., Rodene, E., Yang, J., & Schnable, J. C. (2020). Semantic Segmentation of Sorghum Using Hyperspectral Data Identifies Genetic Associations. *Plant Phenomics*, *2020*, 1–11. https://doi.org/10.34133/2020/4216373

Minervini, M., Scharr, H., & Tsaftaris, S. A. (2015). Image analysis: The new bottleneck in plant phenotyping [applications corner]. *IEEE Signal Processing Magazine*, *32*(4), 126–131. https://doi.org/10.1109/MSP.2015.2405111

Mishra, P., Asaari, M. S. M., Herrero-Langreo, A., Lohumi, S., Diezma, B., & Scheunders, P. (2017). Close range hyperspectral imaging of plants: A review. *Biosystems Engineering*, *164*, 49–67. https://doi.org/10.1016/j.biosystemseng.2017.09.009

Mochida, K., Koda, S., Inoue, K., Hirayama, T., Tanaka, S., Nishii, R., & Melgani, F. (2018). Computer vision-based phenotyping for improvement of plant productivity: A machine learning perspective. *GigaScience*, *8*(1), 1–12. https://doi.org/10.1093/gigascience/giy153

Nagasubramanian, K., Jones, S., Singh, A. K., Sarkar, S., Singh, A., & Ganapathysubramanian, B. (2019). Plant disease identification using explainable 3D deep learning on hyperspectral images. *Plant Methods*, *15*(1), 1–10. https://doi.org/10.1186/s13007-019-0479-8

Neilson, E. H., Edwards, A. M., Blomstedt, C. K., Berger, B., Møller, B. L., & Gleadow, R. M. (2015). Utilization of a high-throughput shoot imaging system to examine the dynamic phenotypic responses of a C4 cereal crop plant to nitrogen and water deficiency over time. *Journal of Experimental Botany*, *66*(7), 1817–1832. https://doi.org/10.1093/jxb/eru526

Pandey, P., Ge, Y., Stoerger, V., & Schnable, J. C. (2017). High throughput in vivo analysis of plant leaf chemical properties using hyperspectral imaging. *Frontiers in Plant Science*, *8*(August), 1–12. https://doi.org/10.3389/fpls.2017.01348

Paproki, A., Sirault, X. R. R., Berry, S., Furbank, R. T., & Fripp, J. (2012). A novel mesh processing based technique for 3D plant analysis. *BMC Plant Biology*, *12*(1), 63. https://doi.org/10.1186/1471-2229-12-63

Paulus, S. (2019). Measuring crops in 3D: Using geometry for plant phenotyping. *Plant Methods*, *15*(1), 1–13. https://doi.org/10.1186/s13007-019-0490-0

Peñuelas, Josep; Filella, I., & Gamon, J. A. (1995). *Assessment of photosynthetic radiation-use. efficiency with spectral reflectance.pdf*. 291–296. https://doi.org/10.1039/c0cc01272f

Pieruschka, R., & Schurr, U. (2019). Plant Phenotyping: Past, Present, and Future. *Plant Phenomics*, *2019*, 1–6. https://doi.org/10.34133/2019/7507131

Pons, T. L., Schieving, F., Hirose, T., & Werger, M. J. A. (1990). Optimization of leaf nitrogen allocation for canopy photoynthesis in Lysmachia vulgaris. In H. Lambers, M. L. Cambridge, H. Konings, & T. L. Pons (Eds.), *Causes and Consequences of Variation in Growth Rate and Productivity of Higher Plants* (pp. 175–186). The Hague: SBP Academic Publishing bv.

Poorter, H., Fiorani, F., Stitt, M., Schurr, U., Finck, A., Gibon, Y., … Pons, T. L. (2012). The art of growing plants for experimental purposes: A practical guide for the plant biologist. *Functional Plant Biology*, *39*(11), 821–838. https://doi.org/10.1071/FP12028

Prusinkiewicz, P. (1998). Modeling of spatial structure and development of plants: A review. *Scientia Horticulturae*, *74*(1–2), 113–149. https://doi.org/10.1016/S0304-4238(98)00084-3

Rapaport, T., Hochberg, U., Rachmilevitch, S., & Karnieli, A. (2014). The effect of differential growth rates across plants on spectral predictions of physiological parameters. *PLoS ONE*, *9*(2), 1–11. https://doi.org/10.1371/journal.pone.0088930

Römer, C., Wahabzada, M., Ballvora, A., Pinto, F., Rossini, M., Panigada, C., … Plümer, L. (2012). Early drought stress detection in cereals: Simplex volume maximisation for hyperspectral image analysis. *Functional Plant Biology*, *39*(11), 878–890. https://doi.org/10.1071/FP12060

Shiraiwa, T., & Sinclair, T. R. (1993). *Distribution of Nitrogen among Leaves in Soybean Canopies Tatsuhiko Shiraiwa and Thomas R . Sinclair * also had an exponential decrease in SLN with relative cumulative leaf area . Only a few data are available to indicate the distribution of SLN in a soyb*. *808*, 804–808.

Sims, D., & Gamon, J. (2002). Relationships between leaf pigment content and spectral reflectance across a wide range of species, leaf structures and developmental stages. *Remote Sensing of Environment*, 337–354. https://doi.org/10.1080/01431161.2017.1399480

Thapa, S., Zhu, F., Walia, H., Yu, H., & Ge, Y. (2018). A novel LiDAR-Based instrument for high-throughput, 3D measurement of morphological traits in maize and sorghum. *Sensors (Switzerland)*, *18*(4). https://doi.org/10.3390/s18041187

Tilling, A. K., O'Leary, G. J., Ferwerda, J. G., Jones, S. D., Fitzgerald, G. J., Rodriguez, D., & Belford, R. (2007). Remote sensing of nitrogen and water stress in wheat. *Field Crops Research*, *104*(1–3), 77–85. https://doi.org/10.1016/j.fcr.2007.03.023

Walter, A., Finger, R., Huber, R., & Buchmann, N. (2017). Smart farming is key to developing sustainable agriculture. *Proceedings of the National Academy of Sciences of the United States of America*, *114*(24), 6148–6150. https://doi.org/10.1073/pnas.1707462114

Wegelin, J. (2000). A survey of Partial Least Squares (PLS) methods, with emphasis on the two-block case. *Technical Report 371*. Seattle: Department of Statistics, University of Washington.

Wold, S., Ruhe, A., Wold, H., & Dunn, W. (1984). The collinearity problem in linear regression. The partial least squared (PLS) approach to generalized inverses. *SIAM Journal on Scientific and Statistical Computing*, *5*, 735–743.

Wold, S., Sjostrom, M., & Eriksson, L. (2001). PLS-regression: a basic tool of chemometrics. *Chemometrics and Intelligent Laboratory Systems*, *58*, 109–130.

Ye, H., Huang, W., Huang, S., Wu, B., Dong, Y., & Cui, B. (2018). Remote estimation of nitrogen vertical distribution by consideration of maize geometry characteristics. *Remote Sensing*, *10*(12), 1–17. https://doi.org/10.3390/rs10121995

Yoder, B. J., & Pettigrew-Crosby, R. E. (1995). Predicting nitrogen and chlorophyll content and concentrations from reflectance spectra (400-2500 nm) at leaf and canopy scales. *Remote Sensing of Environment*, *53*(3), 199–211. https://doi.org/10.1016/0034-4257(95)00135-N

Yuan, Z., Cao, Q., Zhang, K., Ata-Ul-Karim, S. T., Tan, Y., Zhu, Y., … Liu, X. (2016). Optimal leaf positions for SPAD meter measurement in rice. *Frontiers in Plant Science*, *7*(MAY2016), 1–10. https://doi.org/10.3389/fpls.2016.00719

Zarco-Tejada, P. J., Ustin, S. L., & Whiting, M. L. (2005). Temporal and spatial relationships between within-field yield variability in cotton and high-spatial hyperspectral remote sensing imagery. *Agronomy Journal*, *97*(3), 641–653. https://doi.org/10.2134/agronj2003.0257

Zhou, J., Fu, X., Zhou, S., Zhou, J., Ye, H., & Nguyen, H. T. (2019). Automated segmentation of soybean plants from 3D point cloud using machine learning. *Computers and Electronics in Agriculture*, *162*, 143–153. https://doi.org/10.1016/J.COMPAG.2019.04.014